Polyhedron 137 (2017) 222–230

Contents lists available at ScienceDirect

Polyhedron

journal homepage: www.elsevier.com/locate/poly

Kinetics and photophysical behavior of the *P,N*-Re^{I} complex [*P,N*-{$(C_6H_5)_2(C_5H_4N)P$}Re$(CO)_3$(*O*-O_3SCF_3)]: A directly coordinated (and labile) triflate

Gaspar Prado [a], María Belén Ibañez [a,b], Alison Acosta [a], Eduardo Chamorro [a], Patricio Hermosilla-Ibáñez [c], Germán Günther [d], Nancy Pizarro [a], Andrés Vega [a,e,*]

[a] Universidad Andres Bello, Facultad de Ciencias Exactas, Departamento de Ciencias Químicas, Viña del Mar, Chile
[b] Universidad Andres Bello, Escuela de Química y Farmacia, Viña del Mar, Chile
[c] Universidad de Santiago de Chile, Facultad de Química y Biología, Departamento de Química de los Materiales, Chile
[d] Universidad de Chile, Facultad de Ciencias Químicas y Farmacéuticas, Departamento de Química Orgánica y Fisicoquímica, Chile
[e] Centro para el Desarrollo de la Nanociencia y la Nanotecnología, CEDENNA, Chile

ARTICLE INFO

Article history:
Received 9 June 2017
Accepted 18 August 2017
Available online 24 August 2017

Keywords:
Rhenium(I)
Triflate
Labile
Photo-physical
Exchange

ABSTRACT

The reaction of [*P,N*-{$(C_6H_5)_2(C_5H_4N)P$}Re$(CO)_3$Br] (**RePNBr**) with silver triflate leads to the complex [*P,N*-{$(C_6H_5)_2(C_5H_4N)P$}Re$(CO)_3$(*O*-CF_3SO_3)] (**RePNTfO**) with moderate yield. This new *P,N*-Re^{I} triflate compound contains the anion directly coordinated to the metal, completing an octahedral environment. **RePNTfO** displays in dichloromethane (DCM) solution an irreversible oxidation about +1.35 V and three irreversible reduction processes at −1.38 V, −2.03 V and −2.30 V. Oxidation has been attributed to the Re^{I}/Re^{II} couple, while the reduction corresponds to **PN**-ligand processes, which is consistent with those computed by means of DFT. The absorption spectrum of **RePNTfO** in DCM displays a maximum at 295 nm ($\varepsilon = 7.1 \times 10^3$ M^{-1} cm^{-1}) and a shoulder around 350 nm ($\varepsilon = 1.8 \times 10^3$ M^{-1} cm^{-1}), which have been assigned to intraligand ($\pi \rightarrow \pi^*$) and metal to ligand charge transfer (MLCT, $d\pi \rightarrow \pi^*$) transitions with the help of DFT/TDDFT. Excitation of **RePNTfO** in DCM at 350 nm leads to an emission spectrum centered at 535 nm. The analysis of the variation of the absorption and emission spectra in coordinating solvents compared to non-coordinating DCM, DFT/TDDFT calculations modeling and ELF analysis suggests for coordinating solvents that triflate ligand is replaced in the coordination sphere of Re^{I} in solution. Kinetics of the exchange of triflate by bromide measured in DCM at different temperatures allowed to estimate the Eyring parameters: $\Delta H^{\neq}$, $\Delta S^{\neq}$ and $\Delta G^{\neq}$, 50.8 kJ mol^{-1}, −109.6 J K^{-1} mol^{-1} and 83.5 kJ mol^{-1} respectively. The high negative entropy is indicative of a compact transition state, compatible with an associative mechanism, I_a, for the exchange.

1. Introduction

Mononuclear Re^{I} tri-carbonyl complexes having a chelating *P,N*-molecule have been considerably less studied than the corresponding *N,N*-diimines. The presence of a phosphorous atom in the chelating ligand opens new possibilities, due to its trans-effect [1–7]. Described rhenium(I) compounds bearing *P,N*-ligands are almost limited to 2-pyridyldiphenylphosphine, $(C_6H_5)_2(C_5H_4N)P$, with some examples like [{$(C_6H_5)_3P$}{*P,N*-$(C_6H_5)_2(C_5H_4N)P$}Re$(NO)Cl_2$] [8] [{*O,N*-$(C_6H_5)_3P$}{$(C_6H_5)_2(C_5H_4N)PO$}ReCl_3] [9], [{$(C_6H_5)_3P$}{*P,N*-$(C_6H_5)_2(C_5H_4N)P$}Re$(NO)_{0.87}Br_{2.13}$] [10]. In this sense, we have recently reported the synthesis and emission properties of two new Re^{I} compounds, [*P,N*-{$(C_6H_5)_2(C_5H_4N)P$}Re$(CO)_3$Br] (**RePNBr** [11], Scheme 1 left) and [*P,N*-{$(C_6H_5)_2(C_5H_4N)$-NH-P}Re$(CO)_3$Br] (**RePNNBr**) [12]. The **RePNBr** complex shows a low emission quantum yield ($\Phi_{em} < 0.001$) and a biexponential emission decay with luminescence lifetimes in the order of the nanoseconds [11,13]. The analysis lets to conclude that the dual emission observed in such molecule is related to the existence of two excited states associated to the π*-systems on the pyridine and phenyl rings [13]. For **RePNNBr**, the presence of a -NH- bridge between the phosphorous atom and the pyridyl ring allows some additional vibrational modes, making the non-radiative path the favored one. Furthermore, the luminescent emission of this compound comes from ligand centered excited states [12].

* Corresponding author at: Universidad Andres Bello, Facultad de Ciencias Exactas, Departamento de Ciencias Químicas, Viña del Mar, Chile.
E-mail address: andresvega@unab.cl (A. Vega).

http://dx.doi.org/10.1016/j.poly.2017.08.018
0277-5387/

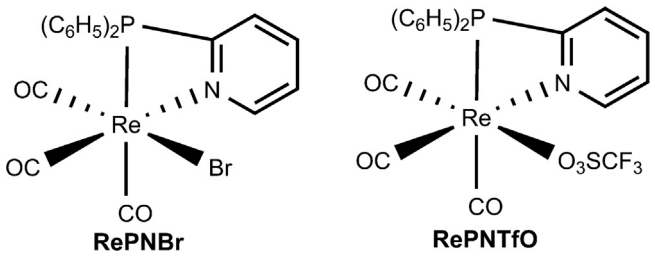

Scheme 1. Structural diagram of [*P,N*-{$(C_6H_5)_2(C_5H_4N)P$}$Re(CO)_3(O\text{-}CF_3SO_3)$] (**RePNTfO**) and its parent complex [*P,N*-{$(C_6H_5)_2(C_5H_4N)P$}$Re(CO)_3Br$] (**RePNBr**).

Maybe the main derivatization path for the Re^I halides in order to produce new compounds with diverse properties goes through the removal of the halide using a silver salt [14]. The reaction between Re^IX compounds with silver salts leads quantitatively to the insoluble (then easily isolable) silver halide. Moreover, the reaction is widely general. Among the silver salts, silver triflate is highly preferred, mainly because of its high solubility in commonly laboratory used organic solvents [15]. Although this fact, structurally described rhenium(I) triflate compounds, according to CSD (v5.36) [16], are very scarce [17–23]. The number of complexes with *P,N* or **P** and **N** ligands is still lower [24,25]. This would be mainly attributed to the interest of the synthetic chemists into the final rhenium compounds rather than into the intermediates. Within the available structure, the position left by the bromide anion upon removal is occupied by solvent molecules or some other available Lewis base, showing, to the best of our knowledge, just one case displaying coordinated triflate [26,27]. In the present work, we focus on the synthesis, structure and the detailed spectroscopic characterization of a new *P,N*-Re^I triflate molecule bearing the anion directly coordinated to the metal, the [*P,N*-{$(C_6H_5)_2(C_5H_4N)P$}$Re(CO)_3(O\text{-}CF_3SO_3)$] (**RePNTfO**, Scheme 1 right) compound. (TD)DFT-calculations of the electronic structure are used to rationalize the structure, while the effect of replacing bromide by triflate is discussed.

2. Experimental

All reagents were used as received from the supplier (Aldrich), with no purification before use. Solvents: dichloromethane (DCM, UvaSol® or *SeccoSolv*® grade, Merck), chloroform ($CHCl_3$, Analysis grade, EMSURE® Merck), acetonitrile (MeCN, Analysis grade, EMSURE® Merck), ethanol (EtOH, Analysis grade, EMSURE® Merck), *N,N*-Dimethylformamide (DMF, Uvasol® grade, Merck), benzene (C_6H_6, Analysis grade, EMSURE® Merck) and toluene (Analysis grade, EMSURE® Merck), were employed as received. Standard Schlenk techniques were used for all manipulations.

2.1. Synthesis

The [*P,N*-{$(C_6H_5)_2(C_5H_4N)P$}$Re(CO)_3(O\text{-}CF_3SO_3)$] (**RePNTfO**) complex was prepared by reaction of the [*P,N*-{$(C_6H_5)_2(C_5H_4N)P$}$Re(CO)_3Br$] (**RePNBr**) complex (prepared according a literature method [11]) with silver triflate according to Scheme 2.

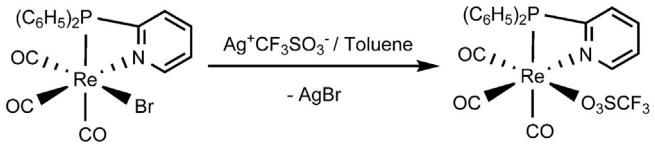

Scheme 2. Synthetic path to **RePNTfO**.

Briefly, to a solution of 800.8 mg of [*P,N*-{$(C_6H_5)_2(C_5H_4N)P$}$Re(CO)_3Br$] (**RePNBr**) (1.305 mmol) in toluene (75 mL) was added to a solution of 335.2 mg of silver triflate (1.305 mmol) in toluene (50 mL), and stirred at room temperature, isolated from light, during 2 h. After reaction, the resulting silver bromide was filtered off. Addition of pentane to this solution leads to precipitation of the complex, allowing the isolation of 492.9 mg of crude **RePNTfO** (55.4% yield). Recrystallization by slow diffusion of pentane to a toluene solution of **RePNTfO** leads to almost transparent and very slightly amber crystals of the compound, which were found suitable for further structural analysis. ***Elemental Analysis:*** Calculated (experimental) for $C_{21}H_{14}F_3NO_6PReS$: C: 36.65% (37.10); H: 2.07% (2.24); N: 2.05% (2.21); S: 4.70% (5.33). FTIR-ATR (major peaks cm^{-1}): $\nu_{C\equiv O}$: 2035, 1912, 1900. ν_{SO}: 1052. ^{1}H-NMR (400 MHz, *d*-$CDCl_3$): δ(ppm) 7.48 (d, 1 H, pyridine), 7.56 (m, 10 H, diphenyl phosphine), 7.65 (t, 1 H, pyridine), 8.02 (t, 1 H, pyridine), 8.84 (d, 1 H, α-proton of pyridine) (see Fig. S1).

2.2. Structural determination

The crystal structure of **RePNTfO** at 293 K was determined by X-ray diffraction on a stick-shaped 0.10 mm × 0.05 mm × 0.05 mm very slightly amber transparent crystal. Data collection was done on a SMART-APEX II CCD diffractometer system. Data was reduced using SAINT [28], while the structure was solved by direct methods, completed by Difference Fourier Synthesis and refined by least-squares using SHELXL [29]. Multi-scan absorption corrections were applied using SADABS [30]. The hydrogen atoms positions were calculated after each cycle of refinement with SHELXL using a riding model for each structure, with C–H distance of 0.93 Å. U_{iso}(H) values were set equal to 1.2 U_{eq} of the parent carbon atom. Table S1 show main data collection and refinement details was prepared with publicif [31].

2.3. Cyclic voltammetry

Cyclic voltammetry studies were performed on a CH-Instruments 650E potentiostat. Cyclic voltammogram at 100 mV s^{-1} at room temperature was recorded in DCM (*SeccoSolv*® Merck) solutions (1.0 mM) using tetrabutylammonium perchlorate (n-Bu_4NClO_4) as the supporting electrolyte (0.1 M). A standard three-electrode cell was used, with a 3-mm diameter glassy carbon working electrode, a platinum wire counter electrode, and an Ag/AgCl coupled with a Luggin capillary reference electrode. All potentials were referred to the redox potential of ferrocene (F_c)/ferrocenium ion (F_c^+) as an internal standard.

2.4. Spectroscopic and photophysical measurements

IR spectrum (4000–400 cm^{-1}) of the compound was measured using a Jasco FTIR-4600 spectrophotometer equipped with an ATR PRO ONE. ^{1}H NMR spectrum was recorded on a Bruker Avance 400 MHz spectrometer at 298 K and using $CDCl_3$ as solvent. UV–Vis spectra were recorded on an Agilent 8453 Diode-Array spectrophotometer in the range of 250–700 nm in aerated solvent solutions at room temperature. Emission spectra were measured in a Horiba Jobin-Yvon FluoroMax-4 spectrofluorometer in different solvents at room temperature or in ethanol-methanol glass (4:1, v/v) at 77 K. Luminescence lifetime measurements were carried out with the time correlated single photon counting technique using a PicoQuant FluoTime300 fluorescence lifetime spectrometer. A subnanosecond Pulsed LED PLS-280 or PLS-300 were employed as pulsed light sources (FWHM ~500 ps; average power 1 μW). Time resolved experiments were made in DCM solutions either air-equilibrated or argon-saturated. Emission quantum yields (Φ_{em}) were measured using procedures described in literature using Quinine

Sulphate in 0.1 M H_2SO_4 or $[Ru(bpy)_3](PF_6)_2$ in acetonitrile solution as standard compounds [32,33]. Singlet oxygen, $O_2(^1\Delta_g)$, measurements were carried out in a Fluotime 200 consisting in a multichannel scaler Nanoharp 200. Excitation at 355 nm was achieved with a laser FTSS355-Q3, (Crystal Laser, Berlin, Germany) working at 1 kHz repetition rate. For the detection at 1270 nm a NIR PMT H10330A (Hamamatsu) was employed. The $O_2(^1\Delta_g)$ quantum yields (Φ_Δ) were determined by comparing the intensity at zero time of the 1270 nm signals to those of optically-matched solutions of phenalelnone as Ref. [34]

2.5. Kinetics and thermodynamic parameters of ligand exchange process

All ligand exchange experiments conducted at different temperature considered the exchange reaction proposed in Scheme 3:

Under conditions $[Br^-] >> [\mathbf{RePNTfO}]$, the observed rate constant, k_{obs}, was assumed to be equal to Eq. (1), where k_0 can be the contribution of an additional pre-dissociative process: [35,36]

$$K_{obs} = k_1[Br^-] + k_0 \quad (1)$$

Following the k_{obs} dependence on the $[Br^-]$, the second order rate constant, k_1, was determined at different temperatures. Using the Eyring Eq. (2):

$$\ln\left(\frac{k_1}{T}\right) = \ln\left(\frac{k_B}{h}\right) + \frac{\Delta S^{\neq}}{R} - \frac{\Delta H^{\neq}}{R}\frac{1}{T} \quad (2)$$

the activation parameters $\Delta S^{\neq}$, $\Delta H^{\neq}$y $\Delta G^{\neq}$ were determined.

2.6. Topological analysis of the electron localization function (ELF)

In order to gain a deeper insight concerning the nature of electron delocalization and bonding in this system, we resort to exploration of the topological analysis of the electron localization function $\eta(r)$ (ELF) [37,38]. The analysis of the gradient vector field of $\eta(r)$ leads directly to a unique division of the molecular space into basins of attractors related to the chemical concepts of structures and bonding. Within such a framework the basins are empirically associated to chemically meaningful concepts such as atomic cores and valence bonding and lone pairs regions. ELF can be interpreted in terms of the relative local excess of kinetic energy density associated to the Pauli principle. ELF is conveniently defined to be ranged in the [0,1] interval, where the highest values correspond to the spatial positions with high relative electron localization. Valence basin densities are naturally delocalized among those associated with the inner atomic shell densities of the core basins. Hence, it is expected that ELF analysis helps to unravel the nature of chemical bonding around the Re center. It should be emphasized however that the ELF electronic basin populations characterize only the spatial organization (not energetically aspects) of the bonding in terms of the electron pair localization [39–41].

2.7. Computational details

All geometry optimizations were performed at the B3LYP/6-31+G(d,p) level of theory using the Gaussian09 Rev C.01 package of programs (G09) [42], and started from geometry determined by means of X-rays diffraction. The LANL2DZ basis set was used only for Rhenium. Excited state calculations were performed within the time-dependent DFT methodology as implemented in G09. Solvent effect for simulating dichloromethane have been incorporated through the polarizable continuum model (PCM) using the integral equation formalism variant (IEFPCM) [43,44]. Absorption and emission spectra were simulated from the above calculations using the GaussSum 3.0 suite of freely available processing tools. A full width at half-maximum (FWHM) of the Gaussian curves corresponding to 3000 cm^{-1} was employed to convolute both spectra. Representations for molecular orbitals were generated using the G09 cubegen tool and have been visualized using VMD and Povray 3.6 programs [45,46]. Topological analyses of $\rho(r)$ and $\eta(r)$ were performed using the TopMod [47] and Multiwfn [48] suite of packages.

$$\mathbf{RePNTfO} + \mathbf{Br^-} \xrightarrow{k_1} \mathbf{RePNBr} + \mathbf{TfO^-}$$

Scheme 3. General reaction for the displacement of triflate by bromide ligand.

3. Results and discussions

3.1. Structural description

The structure of the **RePNTfO** complex is closely related to those of the parent **RePNBr** [11], and can be described as a central Re^I ion octahedrally surrounded by three carbonyl groups in a *fac*-correlation, a chelating and bidentate pyridyl-diphenyl-phosphine (**PN**) molecule and a *O*-coordinated and monodentate triflate, as shown in Fig. 1. The N–Re–P bite angle, 65.67(12)°, is a little bit closer to the value for a regular octahedron (90°) compared to those described for the precursor **RePNBr**, 64.9(1)° [11]. The rhenium to the triflate anion oxygen atoms distances are 2.208(4)Å, 4.235 (6)Å and 3.652(5)Å for O4, O5 and O6 respectively, suggesting the triflate is firmly mono-coordinated to the rhenium atom. Table 1 shows the most significant bond distances and angles. A summary of the most relevant intermolecular interactions is given in Table S2.

3.2. Electrochemistry

Electrochemical properties of **RePNTfO** have been studied by cyclic voltammetry (Fig. 2) and Square-Wave voltammetry (Fig. S2) using DCM and $(N(n\text{-}Bu)_4)^+(ClO_4)^-$ as the supporting electrolyte. All measurements were referred to F_c/F_c^+ potential. The **RePNTfO** complex presents an irreversible peak at around

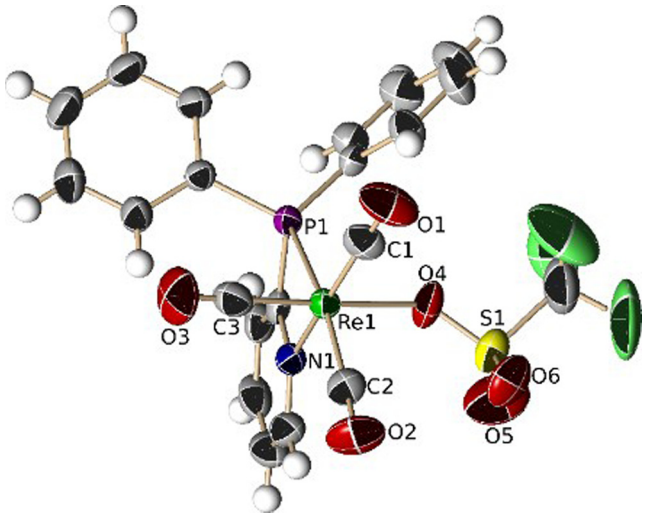

Fig. 1. Molecular structure diagram for **RePNTfO** showing partial atom numbering scheme. Displacement ellipsoids drawn at the 50% level of probability. Hydrogen atoms are drawn as spheres of arbitrary radii.

Table 1
Selected interatomic or bond distances (Å), angles (°) and torsion angles (°) for **RePNTfO**.

Re1–C1	1.901(8)	Re1–N1	2.185(5)
Re1–C2	1.920(7)	Re1–O4	2.208(4)
Re1–C3	1.879(7)	Re1–P1	2.4648(15)
Re1···O5	4.235(6)	Re1···O6	3.652(5)
C1–Re1–C2	89.1(3)	C3–Re1–N1	98.5(2)
C3–Re1–C1	89.5(3)	C2–Re1–O4	96.7(2)
C3–Re1–C2	87.7(3)	N1–Re1–O4	78.62(17)
C1–Re1–N1	167.9(2)	C3–Re1–P1	93.5(2)
C2–Re1–N1	100.2(2)	C1–Re1–P1	105.02(19)
C3–Re1–O4	175.1(2)	C2–Re1–P1	165.8(2)
C1–Re1–O4	92.8(2)	N1–Re1–P1	65.67(12)
S1–O4–Re1	133.7(3)		
Re1–O4–S1–O6	−31.3(5)	Re1–O4–S1–C21	−145.2(5)
Re1–O4–S1–O5	105.9(5)		

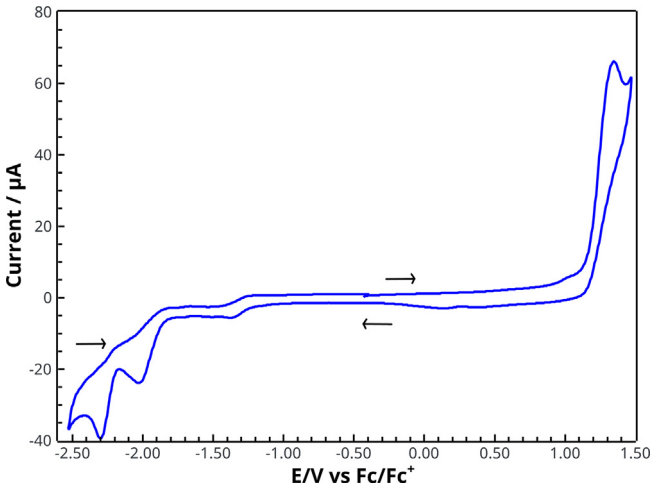

Fig. 2. Cyclic voltammogram of **RePNTfO**, measured in DCM and (n-Bu_4NClO_4) as the supporting electrolyte at scan rate of 100 mV s^{-1}. All measurements were referred to F_c/F_c^+ potential.

+1.35 V, which has been attributed to Re^I/Re^{II} oxidation, as previously reported for **ReNN**, **ReNNN** [49] and **RePNNBr** [12] systems.

Furthermore, the system presents three irreversible reduction processes, with peaks *ca.* at −1.38 V, −2.03 V and −2.30 V, which may be assigned to the stepwise reduction and decomposition of the organic ligand. It has been reported in literature for organometallic complexes containing the diphenyl-2-pyridylphosphine ligand in the structure, that these systems show three irreversible reduction processes at negative potentials [50]. Square-wave voltammetry experiments allowed to visualize and more clearly assign the different oxidation and reduction processes present in the system **RePNTfO**.

By comparison to **RePNBr** and related compounds [13], the last band has been assigned to a ligand reduction. To confirm this proposal, we have optimized the molecular structure of **RePNTfO** by means of DFT calculations. The computed structure in the gas phase closely resembles that determined by X-rays diffraction (Table S3). Vertical oxidation and reduction of the Re^I molecule leads to odd-electron species, where the unpaired electron mainly resides on the rhenium atom in the oxidized specie **RePNTfO$^+$** (Fig. 3a) and into the ligand in the reduced specie **RePNTfO$^-$** (Fig. 3b).

It is interesting to note that upon electron removal or addition, important distortions of the geometry of the corresponding species occur after optimization (Table S3), which is consistent with the observed irreversibility of both waves.

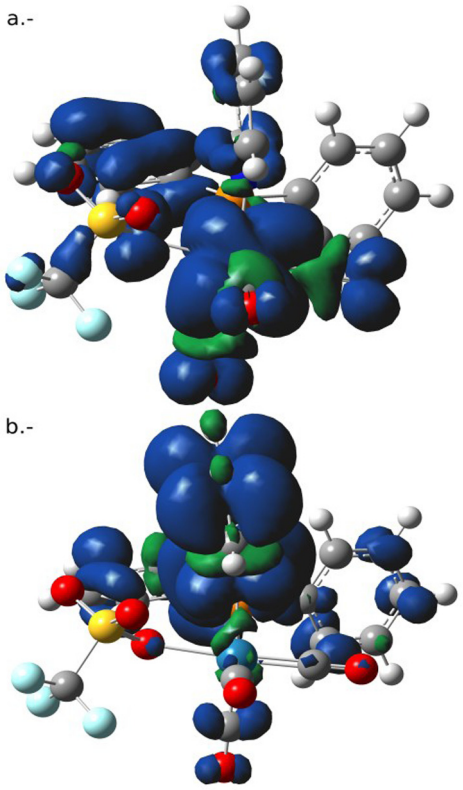

Fig. 3. Gas phase DFT computed spin density transitions for the vertical oxidation (a) and reduction (b) of **RePNTfO**.

3.3. Absorption and emission properties

Fig. 4a shows the absorption spectrum of **RePNTfO** in DCM solution. As can be seen, it has a maximum at 295 nm ($\varepsilon = 7.1 \times 10^3$ M^{-1} cm^{-1}) with a shoulder at 350 nm ($\varepsilon = 1.8 \times 10^3$ M^{-1} cm^{-1}). These absorption bands are typically assigned to intraligand ($\pi \rightarrow \pi^*$) and metal to ligand charge transfer (MLCT, $d\pi \rightarrow \pi^*$) transitions.

For comparison, the absorption spectrum of the parent complex **RePNBr** was also included in Fig. 4a. It can be observed a similar shape of the bands, but an hypsochromic shift occurs when bromide is replaced by triflate.

The displacement of the MLCT band to lower energy in the case of **RePNBr** can be attributed to the retro-back donation effect of the bromide atom orbitals which are contributing to the HOMO orbital. Similar behavior has been reported for homologue NN-diimine coordinated complexes [51,52]. The solvent effect on the absorption band is shown in Fig. 4b.

A bathochromic shift with the polarity can be observed as typically found for MLCT bands, however the band shape lost its structure in more polar solvents. This observation motivates us to explore the possibility of replacement of the coordinated triflate by a solvent molecule, feasible when the solvent has also coordinating capabilities.

Fig. 4c demonstrates the change of the absorption spectra when a small quantity of MeCN is added to a solution of **RePNTfO** in DCM. Similar behavior was found for $[(phen)(H_2O)Re(CO)_3]^+$ (*phen* = 1,10-phenanthroline) [51], where the labile water molecule was proven to be replaced by coordinating solvents.

The emission spectra of **RePNTfO** and **RePNBr** in air-saturated DCM solutions after excitation at 330 nm can be observed in Fig. 5a. The long Stokes Shift is consistent with a MLCT transition. The emission maximum at 535 nm of **RePNTfO** is blue-shifted

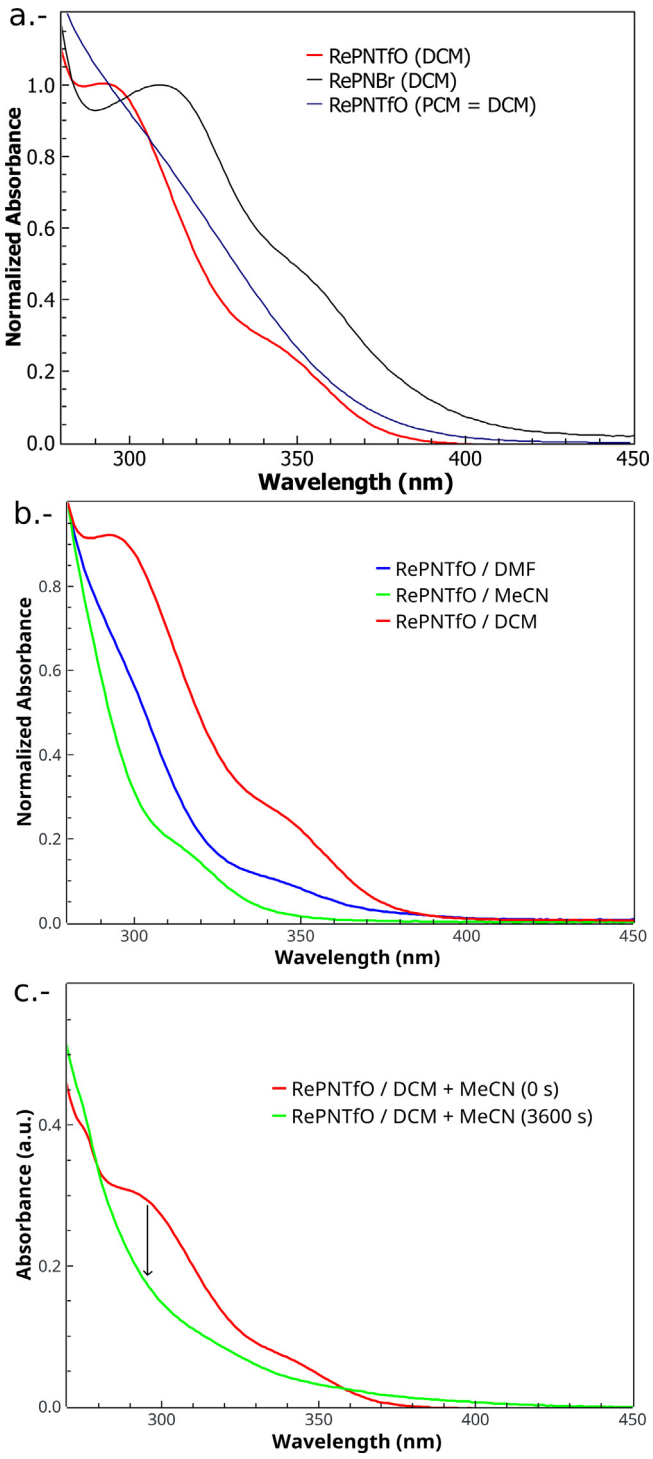

Fig. 4. (a) Absorption spectra of **RePNTfO** and **RePNBr** in DCM. TDDFT computed spectra for **RePNTfO** (PCM = DCM) was included for comparison. (b) Absorption spectra of **RePNTfO** in solvents of different polarities. (c) Spectral absorption change of **RePNTfO** in DCM upon the addition of MeCN.

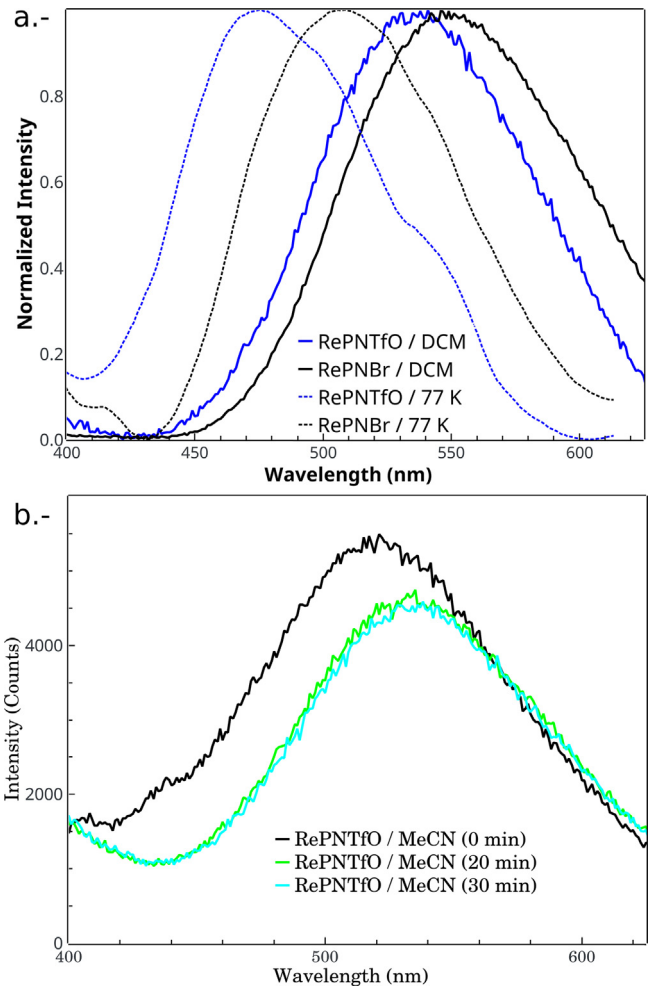

Fig. 5. (a) Emission spectra of **RePNTfO** and **RePNBr** in DCM at room temperature (solid lines) and at 77 K (dotted lines). (b) Time evolution of the emission spectrum of **RePNTfO** in MeCN solution.

when compared with the one of **RePNBr** at 550 nm, which confirms the contribution of bromide orbitals to the HOMO and consistent with bands at lower energies for electron-donor ligands [53]. The structureless emission band of **RePNTfO** in glassy solution at 77 K shows an hypsochromic shift due to the rigidochromic effect previously reported for these kind of complexes [54], remaining at higher energy than its homologue. To confirm the replacement of the triflate group by a solvent molecule, the emission spectra in MeCN solution were recorded following its evolution in time (Fig. 5b). The initial emission band in MeCN solution, centered around 520 nm, exhibits a bathochromic shift attributed to the contribution of the π-acidity of the coordinated molecule of acetonitrile.

Table 2 shows a summary of the photophysical properties of **RePNTfO** measured in diverse solvents. Highly polar or protic ones, like ethanol or DMF, prevented measurement due to emission quenching. As clear from the Table 2 and despite their similar emission spectra (**RePNTfO** and **RePNBr**), the values for emission quantum yields and lifetime are lower when triflate, instead of bromide, is coordinated to rhenium. The highest value for the emission quantum yield; Φ_{em}; was 0.0022, measured in acetonitrile, as would be expected in terms of the Energy-Gap Law [53].

Time resolved experiments allow us to observe a biexponential luminescent decay at 530 nm upon excitation at 300 nm in different solvents. Lifetimes, in the order of a few nanoseconds are measured in some solvents (see Table 2). The amplitude for the long (τ_1) and short (τ_2) components show a slight dependence with the solvent nature. These results evidence the presence of two emissive excited states, as previously described for **RePNBr** [13].

For this last complex, the biexponential decay was related to the presence of two different MLCT triplet excited states very close in energy, one of those involving the pyridine orbitals ($d_\pi \rightarrow \pi^*_{py}$) and the other one, the phenyl ones ($d_\pi \rightarrow \pi^*_{ph}$) [13]. It seems that

Table 2
Summary of the photophysical properties of **RePNTfO** in air equilibrated solvent solutions.[a]

Solvent	λ_{abs} (nm) ($\varepsilon/10^3$ M^{-1} cm^{-1})	λ_{em} (nm)	Φ_{em}	τ[b] (ns)	Φ_{Δ}
DCM	295 (7.1) 350 (1.8)	535	0.0012	11.6 (14%) 2.6 (86%)	0.020
C_6H_6	296 (5.0) 350 (1.9)	530	0.0013	7.89 (27%) 0.93 (73%)	0.032
MeCN	280 (5.1) 315 (1.0)	520	0.0022	21.5 (90%) 0.73 (10%)	–
DMF	290 (6.9) 340 (1.2)	540	<0.0010	–	–
EtOH	296 (3.5) 330 (1.3)	520	<0.0010	–	–

[a] Errors were lower than 10%.
[b] Values reported between parentheses are amplitudes in percent contribution from each decay component.

this characteristic is preserved for **RePNTfO**, just with shorter lifetimes probably due to the presence of the triflate ligand. As we excited at 300 nm, it is probably too, that the short component can be related to an intraligand transition. The triplet character for the emissive states was stated by measuring the singlet oxygen generation.

3.4. Computational calculations

To get a deeper understanding of the photophysical behavior related to its electronic structure, we have performed DFT/TD-DFT modeling for the **RePNTfO** compound, and for the hypothetic compounds **RePNMeCN**$^+$ and **RePNDMF**$^+$ (see Scheme 4), where triflate has been replaced by MeCN and DMF respectively. For each case, calculations have been made in the gas phase and using the corresponding PCM. The idea is to test the effect on the absorption spectra of the solvent polarity and the triflate substitution for a solvent molecule, as suggested by photo-physical results.

Table S3 shows the main optimized distances for **RePNTfO**, **RePNMeCN**$^+$ and **RePNDMF**$^+$, in good agreement with X-rays determined values for **RePNTfO**. Table 3 shows the TDDFT computed excitations for **RePNTfO** in the gas phase, while Fig. 6 depicts the DFT computed frontier orbitals HOMO−1, HOMO, LUMO and LUMO+1. A complete DFT computed frontier orbitals for **RePNTfO**, **RePNMeCN**$^+$ and **RePNDMF**$^+$ can be found in supplementary information Fig. S3.

These results support that the lowest energy transition involve a charge transfer from the metal to the ligand π^*-orbitals, confirming the MLCT nature attributed by the photophysical results to the absorption centered at 350 nm, while the higher energy transitions involve ligand orbitals and have $\pi \rightarrow \pi^*$ character. TDDFT results show the ^{1}MLCT band computed for **RePNTfO** should suffer hypsochromic shift with solvent polarity, as clear from Fig. S4a. As proposed before, coordinating solvents like MeCN or even DMF could replace labile groups in Re^I complexes [51].

To compute the potential effect in the absorption spectra of the replacement of the triflate in the rhenium first coordination sphere, Fig. S4b shows the TDDFT computed spectra in the gas phase for **RePNTfO**, **RePNMeCN**$^+$ and **RePNDMF**$^+$. Weakly coordinating DMF has similar effect than the triflate, but MeCN should produce a strong influence on the absorption spectra, especially in the MLCT band. Fig. S4c shows the TDDFT computed spectra for **RePNMeCN**$^+$ in the PCM model for MeCN and for **RePNDMF**$^+$ in the PCM model for DMF, while Table S4 shows a detail of the excitations for each model. DFT/TDDFT results strongly support the hypothesis of substitution of the triflate anion by the ligand in the Re^I coordination sphere in solution.

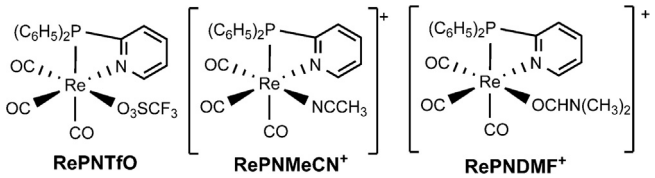

Scheme 4. Schematic drawings of the structure of **RePNTfO** and the model compounds **RePNMeCN**$^+$ and **RePNDMF**$^+$.

3.5. ELF characterization of chemical bonding in RePNTfO

The topological analysis of ELF provides a picture of bonding in terms of electron pair regions. The ELF analysis (Figs. 7and 8) evidences that there is no disynaptic basin associated to the region between the Re1 center and the O4 atom of the triflate. In contrast, five well defined valence disynaptic basins are located in the coordinating sphere around the Re center, i.e., V(Re1, N1), V(Re1, P1), V (Re1, C1), V(Re1, C2), and V(Re1, C3), which integrates 2.62e, 1.92e, 3.06e, 2.92e, and 3.19e respectively. ELF highlights the common distorted octahedral coordination sphere of Re(I). It became clear that the valence region around the Re center interacts with the nonbonding (lone pair) region of the O4 oxygen which integrates to 6.08e. The Re–O4 can be associated in such a framework to a more labile interaction than those characterizing the Re–CO bonds Fig. 9.

3.6. Triflate exchange kinetics

To have a direct proof of triflate exchange, we tried reaction of **ReNTfO** with tetrabuthylammonium bromide in solution, since the exchange leads to the well characterized product **RePNBr** [13], and to gain detailed knowledge of the process. Kinetic experiments of triflate exchange by bromide at different temperatures would also provide information about the reaction mechanism.

Considering the reaction in Scheme 3 and fulfilment the condition [Br^-] >> [**RePNTfO**], the changes of the absorption were followed as shown in Fig. 7.

The Inset corresponds to the lineal dependence of the observed rate constant, k_{obs}, on the bromide concentration in DCM at 20 °C. From the slope of this plot, the bimolecular rate constant, k_1, was obtained. These values at different temperatures (see Table 4), allow us to get the Eyring parameters.

As can be seen from the absorption band In our case, the presence of the *P,N*-ligand and also, the nucleophilicity of the bromide, contribute to the easy replacement of the triflate. In addition, the good ability as leaving moiety of triflate, can be related to the activation parameters, with a high negative value for $\Delta S^{\neq}$, being around 40% of contribution to $\Delta G^{\neq}$. This major entropic factor could be explained in terms of more order and compact transition state, which is compatible with an associative mechanism, I_a.

Table 3
Summary of main energy, wavelength and oscillator strength computed for observed transitions in the absorption spectra of **RePNTfO** in gas phase.

N	*E* (eV)	λ (nm)	*f*	Major contributions
1	3.37	368	0.021	HOMO−1 → LUMO (11%) HOMO → LUMO (88%)
2	3.46	358	0.011	HOMO−1 → LUMO (88%) HOMO → LUMO (10%)
4	3.77	329	0.021	HOMO → LUMO+1 (83%)
5	3.90	318	0.038	HOMO−1 → LUMO+1 (83%)
10	4.24	292	0.034	HOMO−3 → LUMO (93%)

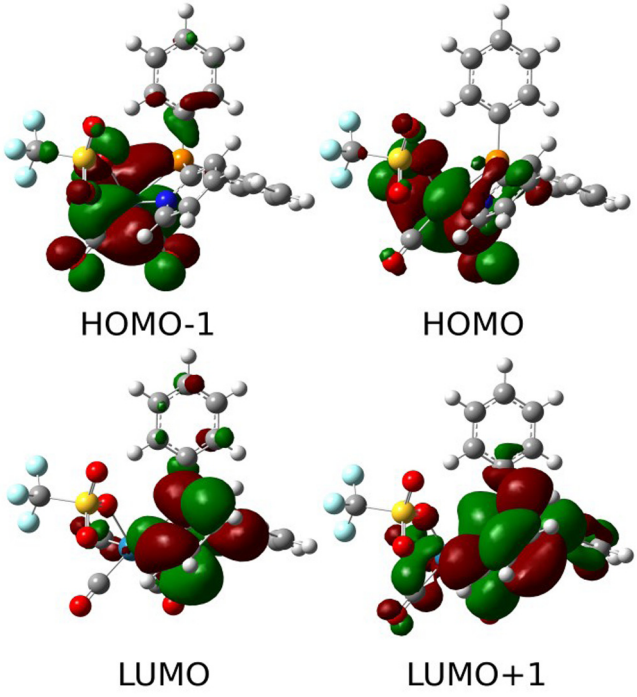

Fig. 6. DFT computed frontier orbitals HOMO−1, HOMO, LUMO and LUMO+1 plots for **RePNTfO**. A complete set can be found in electronic supplementary information.

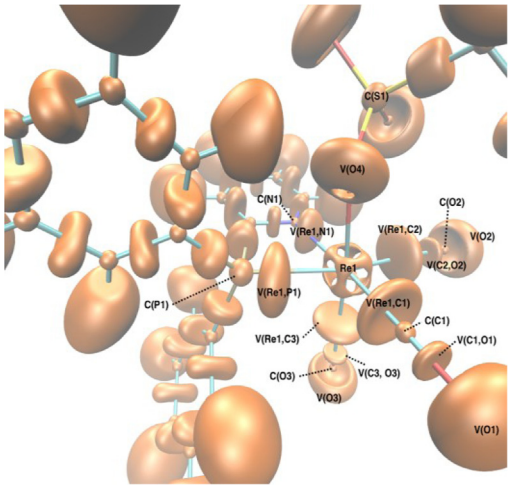

Fig. 7. View of the ELF = 0.836 isosurface for **RePNTfO**. The region between the Re1 and O4 centers do not exhibit a disynaptic basin.

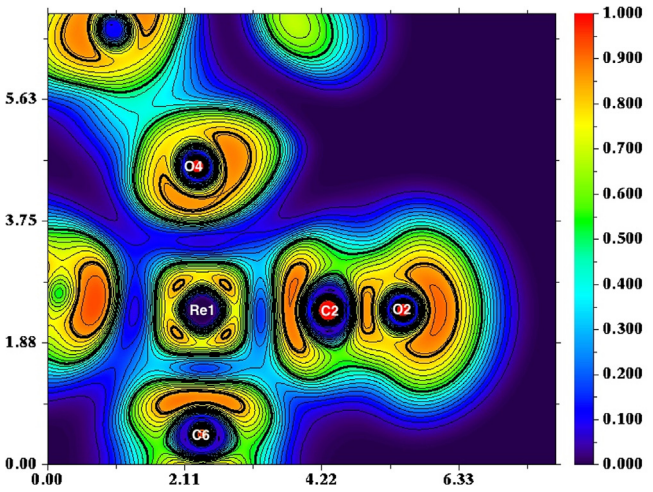

Fig. 8. ELF color-filled map with contour lines for **RePNTfO** in a plane defined by the O1–Re1–O4 atomic cores. Bolded lines correspond to ELF = 0.836 (inner) and ELF = 0.500 (outer). Length unit is Angstrom.

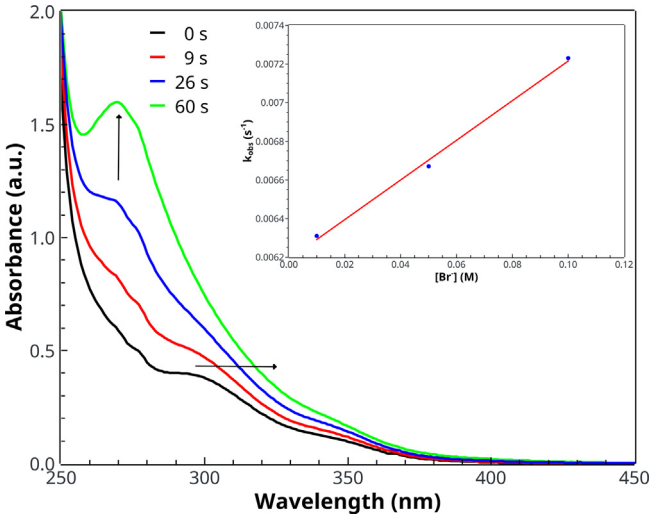

Fig. 9. Time evolution of the absorption spectrum for the reaction of **RePNTfO** with Br^-. ***Inset:*** Determination of the rate constant, k_1, from plot of k_{obs} vs [Br^-] in DCM at 20 °C.

4. Conclusions

The reaction of [*P,N*-{$(C_6H_5)_2(C_5H_4N)P$}Re$(CO)_3$Br] (**RePNBr**) with silver triflate produces the [*P,N*-{$(C_6H_5)_2(C_5H_4N)P$}Re$(CO)_3$(*O*-CF_3SO_3)] (**RePNTfO**), which contains the anion directly coordinated to Re^I. **RePNTfO** experiences one irreversible oxidation at +1.35 V (Re^I/Re^{II}) couple and three irreversible reduction processes at −1.38 V, −2.03 V and −2.30 V (*P,N*-ligand). The complex in DCM solution displays a maximum at 295 nm and a shoulder around 350 nm, which corresponds to intraligand ($\pi \rightarrow \pi^*$) and metal to ligand charge transfer (MLCT, $d\pi \rightarrow \pi^*$). Excitation of **RePNTfO** in DCM at 350 nm leads to an emission spectrum centered at 535 nm. The change of the absorption and emission spectra in coordinating solvents compared to those observed in non-coordinating ones together with DFT/TDDFT calculations suggests that coordinating solvents replace the triflate into the coordination sphere of Re^I in solution. ELF analysis confirms a very weak bond between Re^I and triflate oxygen atom. Kinetics of the exchange of triflate by bromide measured in DCM at different temperatures

Table 4
Rate constants and activation parameters from Eyring plot for the forward reaction of **RePNTfO** with bromide (Br^-).

k_1 (10^{-3} M^{-1} s^{-1})*		Eyring parameters		
20 °C	40 °C	$\Delta H^{\neq}$ (kJ mol^{-1})*	$\Delta S^{\neq}$(J mol^{-1} K^{-1})*	$\Delta G^{\neq}$ (kJ mol^{-1})*
10.2	41.1	50.8	−109.6	83.5

* Errors were lower than 10%.

allowed to estimate the Eyring parameters: $\Delta H^{\neq}$, $\Delta S^{\neq}$ and $\Delta G^{\neq}$, 50.8 kJ mol^{-1}, −109.6 J K^{-1} mol^{-1} and 83.5 kJ mol^{-1} respectively. The high negative entropy is indicative of a compact transition state, compatible with an associative mechanism, I_a, for the exchange.

Acknowledgements

The authors gratefully acknowledge partial financial support of Comisión Nacional Científica y Tecnológica, grants FONDECYT 1160546, 1160749, ACT-1404 (IPMaG) and UNAB DI-1253-16/R. AV is a member of Financiamiento Basal para Centros Científicos y Tecnológicos de Excelencia FB0807.

Appendix A. Supplementary data

CCDC 1504763 contains the supplementary crystallographic data for [*P,N*-{$(C_6H_5)_2(C_5H_4N)P$}$Re(CO)_3$(*O*-CF_3SO_3)]. These data can be obtained free of charge via http://dx.doi.org/10.1016/j.poly.2017.08.018, or from the Cambridge Crystallographic Data Centre, 12 Union Road, Cambridge CB2 1EZ, UK; fax: (+44) 1223-336-033; or e-mail: deposit@ccdc.cam.ac.uk. Experimental and computed bond distances for the [*P,N*-{$(C_6H_5)_2(C_5H_4N)P$}$Re(CO)_3$(*O*-CF_3SO_3)]$^+$ and [*P,N*-{$(C_6H_5)_2(C_5H_4N)P$}$Re(CO)_3$(*O*-CF_3SO_3)]. Supplementary data associated with this article can be found, in the online version, at http://dx.doi.org/10.1016/j.poly.2017.08.018.

References

[1] P. Braunstein, Functional ligands and complexes for new structures, homogeneous catalysts and nanomaterials, J. Organomet. Chem. 689 (2004) 3953.
[2] P. Braunstein, F. Naud, Hemilability of hybrid ligands and the coordination chemistry of oxazoline-based systems, Angew. Chem., Int. Ed. 40 (2001) 680.
[3] P. Espinet, K. Soulantica, Phosphine-pyridyl and related ligands in synthesis and catalysis, Coord. Chem. Rev. 193–195 (1999) 499.
[4] P.J. Guiry, C.P. Saunders, The development of bidentate P,N ligands for asymmetric catalysis, Adv. Synth. Catal. 346 (2004) 497.
[5] G. Helmchen, A. Pfaltz, Phosphinooxazolines a new class of versatile, modular P,N-ligands for asymmetric catalysis, Acc. Chem. Res. 33 (2000) 336.
[6] G.R. Newkome, Pyridylphosphines, Chem. Rev. 93 (1993) 2067.
[7] A. Pfaltz, W.J. Drury, Design of chiral ligands for asymmetric catalysis: From C2-symmetric P,P- and N,N-ligands to sterically and electronically nonsymmetrical P,N-ligands, Proc. Natl. Acad. Sci. U.S.A. 101 (2004) 5723.
[8] B. Machura, R. Kruszynski, Synthesis, crystal, molecular and electronic structure of the [$Re(NO)Cl_2(PPh_3)$(PPh_2py-P,N)] complex, Polyhedron 25 (2006) 1985.
[9] B. Machura, A. Jankowska, R. Kruszynski, J. Kłak, J. Mroziński, Structural and spectroscopic studies on rhenium(III) diphenyl(2-pyridyl)phosphine oxide complexes, Polyhedron 25 (2006) 2663.
[10] B. Machura, R. Kruszynski, Synthesis, crystal, molecular and electronic structure of the [$Re(NO)_{0.87}Br_{2.13}(PPh_3)$($PPh_2$py-P,N)] complex and DFT calculations of [$Re(NO)Br_2(PPh_3)$(PPh_2py-P,N)], J. Mol. Struct. 837 (2007) 92.
[11] F. Venegas, N. Pizarro, A. Vega, Structural and Photophysical properties of a mononuclear Re(I) complex:[P,N-{$(C_6H_5)_2(C_5H_5N)P$}$Re(CO)_3Br$], J. Chil. Chem. Soc. 56 (2011) 823.
[12] P. Mella, J.C. Palma, M. Cepeda-Plaza, P. Aguirre, J. Manzur, G. Günther, N. Pizarro, A. Vega, Tuning the photophysical properties of a (P,N)Re^I complex by adding a –NH– fragment into a P,N-bidentate ligand: The case of [P,N-{$(C_6H_5)_2(C_5H_4N)NHPRe(CO)_3Br$], Polyhedron 111 (2016) 64.
[13] N. Pizarro, M. Duque, E. Chamorro, S. Nonell, J. Manzur, J.R. de la Fuente, G. Gunther, M. Cepeda-Plaza, A. Vega, Dual Emission of a Novel (P,N)Re(I) Complex: A Computational and Experimental Study on [*P,N*-{$(C_6H_5)_2(C_5H_4N)P$}$Re(CO)_3Br$], J. Phys. Chem. A 119 (2015) 3929.
[14] K.D. Benkstein, J.T. Hupp, C.L. Stern, Molecular rectangles based on rhenium(i) coordination chemistry, J. Am. Chem. Soc. 120 (1998) 12982.
[15] T. Howard Black, Silver(I) trifluoromethanesulfonate, in: Encyclopedia of Reagents for Organic Synthesis, John Wiley & Sons Ltd, 2001.
[16] I.J. Bruno, J.C. Cole, P.R. Edgington, M. Kessler, C.F. Macrae, P. McCabe, J. Pearson, R. Taylor, New software for searching the Cambridge Structural Database and visualizing crystal structures, Acta Crystallogr., Sect. B 58 (2002) 389.
[17] M. Casanova, E. Zangrando, F. Munini, E. Iengo, E. Alessio, *fac*-[$Re(CO)_3$(dmso-$O)_3$](CF_3SO_3): a new versatile and efficient Re(I) precursor for the preparation of mono and polynuclear compounds containing fac-[$Re(CO)_3$]$^+$ fragments, Dalton Trans. (2006) 5033.
[18] W.B. Connick, A.J. Di Bilio, M.G. Hill, J.R. Winkler, H.B. Gray, Tricarbonyl(1,10-phenanthroline) (imidazole) rhenium(I): a powerful photooxidant for investigations of electron tunneling in proteins, Inorg. Chim. Acta 240 (1995) 169.
[19] M. Espinal Viguri, M.A. Huertos, J. Pérez, L. Riera, I. Ara, Re-mediated C–C coupling of pyridines and imidazoles, J. Am. Chem. Soc. 134 (2012) 20326.
[20] M.A. Huertos, J. Pérez, L. Riera, J. Díaz, R. López, From bis(N-alkylimidazole) to bis(NH–NHC) in rhenium carbonyl complexes, Angew. Chem., Int. Ed. 49 (2010) 6409.
[21] T. Jurca, O. Ramadan, I. Korobkov, D.S. Richeson, Employing sterically encumbered bis(imino)pyridine ligands in support of fac-rhenium(I) carbonyls, J. Organomet. Chem. 802 (2016) 27.
[22] B. Salignac, P.V. Grundler, S. Cayemittes, U. Frey, R. Scopelliti, A.E. Merbach, R. Hedinger, K. Hegetschweiler, R. Alberto, U. Prinz, G. Raabe, U. Kölle, S. Hall, Reactivity of the organometallic fac-[$(CO)_3Re^I(H_2O)_3$]$^+$ aquaion. Kinetic and thermodynamic properties of H_2O substitution, Inorg. Chem. 42 (2003) 3516.
[23] M.E. Viguri, J. Pérez L. Riera, C–C coupling of N-heterocycles at the fac-$Re(CO)_3$ fragment: synthesis of pyridylimidazole and bipyridine ligands, Chem. Eur. J. 20 (2014) 5732–5740.
[24] M.A.C. Rodríguez, J. Bravo, E. Freijanes, E. Oñate, G.A.-F. Soledad, P. Rodríguez-Seoane, Synthesis and reactivity of [$Re(ClCH_2Cl)(CO)_3L$][A] and [$Re(OSO_2CF_3)$ $(CO)_3L$] (L = $Ph_2PO(CH_2)_2OPPh_2$; A = BF_4, [B{3,5-$(CF_3)_2C_6H_3$}$_4$]): the crystal structure of [$Re(OSO_2CF_3)(CO)_3L$] and [$Re(NCCH_3)(CO)_3L$][BF_4], Polyhedron 23 (2004) 1045–1053.
[25] D. Veghini, H. Berke, The nitrosyl ligand and the rhenium–triflate bond in rhenium(I) complexes, Inorg. Chem. 35 (1996) 4770.
[26] P. Gómez-Iglesias, M. Arroyo, S. Bajo, C. Strohmann, D. Miguel, F. Villafañe, Pyrazolylamidino ligands from coupling of acetonitrile and pyrazoles: a systematic study, Inorg. Chem. 53 (2014) 12437.
[27] L.L. Ouh, T.E. Müller, Y.K. Yan, Intramolecular hydroamination of 6-aminohex-1-yne catalyzed by Lewis acidic rhenium(I) carbonyl complexes, J. Organomet. Chem. 690 (2005) 3774.
[28] M. SAINTPLUS V6.22 Bruker AXS Inc., WI, USA.
[29] G.M.S.N.V. Sheldrick, Bruker AXS Inc., Madison, WI, USA, 2000.
[30] W. SADABS V2.05 Bruker AXS Inc., Madison, USA.
[31] S. Westrip, PublCIF: software for editing, validating and formatting crystallographic information files, J. Appl. Crystallogr. 43 (2010) 920.
[32] G.A. Crosby, J.N. Demas, Measurement of photoluminescence quantum yields. Review, J. Phys. Chem. 75 (1971) 991.
[33] K. Suzuki, A. Kobayashi, S. Kaneko, K. Takehira, T. Yoshihara, H. Ishida, Y. Shiina, S. Oishi, S. Tobita, Reevaluation of absolute luminescence quantum yields of standard solutions using a spectrometer with an integrating sphere and a back-thinned CCD detector, Phys. Chem. Chem. Phys. 11 (2009) 9850.
[34] R. Schmidt, C. Tanielian, R. Dunsbach, C. Wolff, Phenalenone, a universal reference compound for the determination of quantum yields of singlet oxygen $O_2(^1\Delta_g)$ sensitization, J. Photochem. Photobiol., A 79 (1994) 11.
[35] A. Roodt, J.G. Leipoldt, E.A. Deutsch, J.C. Sullivan, Kinetic and structural studies on the oxotetracyanotechnetate(V) core: protonation and ligation of dioxotetracyanotechnetate(V) ions and crystal structure of 2,2′-bipyridinium trans-oxothiocyanatotetracyanotechnetate(V), Inorg. Chem. 31 (1992) 1080.
[36] H.J. van der Westhuizen, R. Meijboom, M. Schutte, A. Roodt, Mechanism for the formation of substituted manganese(V) cyanidonitrido complexes: crystallographic and kinetic study of the substitution reactions of trans-[$MnN(H_2O)(CN)_4$]$^{2-}$ with monodentate pyridine and bidentate pyridine–carboxylate ligands, Inorg. Chem. 49 (2010) 9599.
[37] A. Savin, B. Silvi, F. Colonna, Topological analysis of the electron localization function applied to delocalized bonds, Can. J. Chem. 74 (1996) 1088.
[38] B. Silvi, A. Savin, Classification of chemical bonds based on topological analysis of electron localization functions, Nature 371 (1994) 683.
[39] E. Chamorro, P. Fuentealba, A. Savin, Electron probability distribution in AIM and ELF basins, J. Comput. Chem. 24 (2003) 496.
[40] L. Lopez, P. Ruiz, M. Castro, J. Quijano, M. Duque-Norena, P. Perez, E. Chamorro, Understanding the thermal dehydrochlorination reaction of 1-chlorohexane. Revealing the driving bonding pattern at the planar catalytic reaction center, RSC Adv. 5 (2015) 62946.

[41] L.R. Domingo, M. Ríos-Gutiérrez, P. Pérez, E. Chamorro, Understanding the [2n + 2n] reaction mechanism between a carbenoid intermediate and CO_2, Mol. Phys. 114 (2016) 1374.
[42] M.J.T. Frisch, G.W. Schlegel, H.B. Scuseria, G.E. Robb, M.A. Cheeseman, J.R. Scalmani, G. Barone, V. Mennucci, B. Petersson, G.A. Nakatsuji, H. Caricato, et al., Gaussian 09, Gaussian Inc, Wallingford CT, 2009.
[43] S. Miertuš, E. Scrocco, J. Tomasi, Electrostatic interaction of a solute with a continuum. A direct utilizaion of AB initio molecular potentials for the prevision of solvent effects, Chem. Phys. 55 (1981) 117.
[44] S. Miertus~, J. Tomasi, Approximate evaluations of the electrostatic free energy and internal energy changes in solution processes, Chem. Phys. 65 (1982) 239–245.
[45] Persistence of Vision Pty. Ltd., Persistence of Vision Raytracer (Version 3.6) [Computer software], 2004. Retrieved from: <http://www.povray.org>.
[46] W. Humphrey, A. Dalke, K. Schulten, VMD: visual molecular dynamics, J. Mol. Graphics 14 (1996) 33.
[47] S. Noury, X. Krokidis, F. Fuster, B. Silvi, Computational tools for the electron localization function topological analysis, Comput. Chem. 23 (1999) 597.
[48] T. Lu, F. Chen, Multiwfn: a multifunctional wavefunction analyzer, J. Comput. Chem. 33 (2012) 580.
[49] M.R. Gonçalves, K.P.M. Frin, Synthesis, characterization, photophysical and electrochemical properties of fac-tricarbonyl(4,7-dichloro-1,10-phenanthroline)rhenium(I) complexes, Polyhedron 97 (2015) 112.
[50] P. Kumar, A.K. Singh, M. Yadav, P.-Z. Li, S.K. Singh, Q. Xu, D.S. Pandey, Synthesis and characterization of ruthenium(II) complexes based on diphenyl-2-pyridylphosphine and their applications in transfer hydrogenation of ketones, Inorg. Chim. Acta 368 (2011) 124.
[51] P. Mella, K. Cabezas, C. Cerda, M. Cepeda-Plaza, G. Gunther, N. Pizarro, A. Vega, Solvent, coordination and hydrogen-bond effects on the chromic luminescence of the cationic complex $[(phen)(H_2O)Re(CO)_3]^+$, New J. Chem. 40 (2016) 6451.
[52] M. Schutte, G. Kemp, H.G. Visser, A. Roodt, Tuning the reactivity in classic low-spin d6 rhenium(i) tricarbonyl radiopharmaceutical synthon by selective bidentate ligand variation (L,L′-Bid; L,L′ = N,N′, N,O, and O,O′ donor atom sets) in fac-$[Re(CO)_3(L,L'\text{-Bid})(MeOH)]_2$ complexes, Inorg. Chem. 50 (2011) 12486.
[53] J.V. Caspar, T.J. Meyer, Application of the energy gap law to nonradiative, excited-state decay, J. Phys. Chem. 87 (1983) 952.
[54] M. Wrighton, D.L. Morse, Nature of the lowest excited state in tricarbonylchloro-1,10-phenanthrolinerhenium(I) and related complexes, J. Am. Chem. Soc. 96 (1974) 998.